Moroccan Journal of Chemistry
ISSN : 2351-812X

Mor. J. Chem., 2024, Volume 12, Issue 1, Page 145-156
https://revues.imist.ma/index.php/morjchem
https://doi.org/10.48317/IMIST.PRSM/morjchem-v12i1.43797

Effect of Calcium/phosphorus Ratio on the Chemical and Structural Properties of Oxygenated Apatite Synthesized by Neutralization

Jerdioui S. [1*], Elansari L. L. [1], Bouammali H. [1], Azzaoui K. [2], Sabbahi R. [3], Hammouti B. [4,5], Mejdoubi M. [1]

[1]Laboratory of Applied Chemistry and Environment (LCAE), Department of Chemistry, Faculty of Sciences, Mohamed I University, P.O. Box 717, 60000 Oujda, Morocco
[2] Laboratory of Engineering, Electrochemistry, Modelling and Environment, Faculty of Sciences, Sidi Mohamed Ben Abdellah University, 30000 Fez, Morocco
[3] Higher School of Technology, Ibn Zohr University, P.O. Box 3007, Laayoune, Morocco
[4] Euro-Mediterranean University of Fes, P.O. Box 15, 30070 Fez, Morocco
[4] Laboratory of Industrial Engineering, Energy and The Environment (LI3E) SUPMTI Rabat, Morocco
**Corresponding author, Email address: souhailjjerdioui0@gmail.com*

Received *24 Sept 2023,*
Revised *04 Nov 2023,*
Accepted *07 Nov 2023*

Citation*: Jerdioui S., Elansari L. L., Bouammali H., Azzaoui K., Sabbahi R., Hammouti B., Mejdoubi M. (2024) Effect of calcium/phosphorus ratio on the chemical and structural properties of oxygenated apatite synthesized by neutralization Mor. J. Chem., 12(1), 145-156*

Abstract: Zinc oxide-based cements are commonly used to fill dental canals, but they have drawbacks such as poor bonding and bacterial infection. In this work, we propose a novel phosphocalcic apatitic cement/oxygenated apatite mixture, which can mimic the natural filling of dental canals. Oxygenated apatite is a type of apatite that contains molecular oxygen in their tunnels. We aim to evaluate the effect of the Calcium/Phosphorus (Ca/P) atomic ratio on the chemical and structural properties of the synthesized oxygenated apatite, as well as on the quantity of oxygen retained in their tunnels. We use the neutralization method to precipitate apatite from lime milk and orthophosphoric acid, in the presence of hydrogen peroxide. We characterize the materials the materials by X-ray diffraction, infrared absorption spectroscopy, thermal analysis, adsorption-desorption of nitrogen, and elemental analysis. We obtain simple oxygenated apatitic phases with a Ca/P ratio ranging from 1.53 to 1.76, an oxygen insertion rate of $3.5x10^{-4}$ moles, and a chemical formula of $Ca_{9,9}(PO_4)_6(OH)_2(O_2)_{0,69}(CO_2)_{0,01}$. We find that the deviation from stoichiometry and calcination at 900°C leads to the formation of a biphasic mixture of PAH/β-TCP. The synthesized apatites have low crystallinity and high specific surface area, which decreases from 156.3 to 141.6 m^2/g as the Ca/P ratio increases.

Keywords: Adsorption-desorption isotherms; antiseptic; dissolution-reprecipitation; oxygenated apatite (OA); Neutralization.

Abbreviations
BET : Brunaur, Emmett, Teller
BJH : Barret, Joyner, Halenda
β-TCP : β-Tricalcium phosphate
Ca/P: Calcium/Phosphorus
DDS: Drug delivery system
Dp : Pore diameter
HAp : Hydroxyapatite
FTIR : Transform infrared spectroscopy
ICP–AES : Inductively Coupled Plasma – Atomic Emission Spectrometry
OA: Oxygenated apatite
SEM : Scanning electron microscopy
IUPAC : International Union of Pure and Applied Chemistry
SS : Specific surface
TGA : Thermogravimetric analysis
TDA : Thermal differential analysis
XRD : X-ray diffraction
Vp : Pore volume

1. Introduction

Phosphocalcic apatitic biomaterials have great potential in the medical field, particularly in orthopedics and dental implant coatings due to their similarity to the mineral part of bone, their low solubility, and their excellent biocompatibility, osteoinduction, and osteoconduction properties (Hammari *et al.* 2022; Fiume *et al.*, 2021; Dorozhkin *et al.*, 2019; Raquel Maia *et al.*, 2019; Siddiqui *et al.*, 2018; Akartasse *et al* 2017). It is necessary to develop the elaboration of the apatites having interesting reactivity to improve their physicochemical and biological properties (Aaddouz *et al.*, 2023; Saidi *et al.*, 2022; Errich *et al.*, 2021; Vandecandelaere *et al.*, 2013). Indeed, work has been carried on the elaboration of mineral-organic apatites. In this axis, a precipitation reaction was carried out between a mineral phosphate and an organic phosphate (amino-2 ethyl- phosphate), which made it possible to obtain composites having interesting biomedical applications (Subirade *et al.*, 1991) (Subirade *et al.*, 1993). The adsorption of proteins on apatites has been widely studied in recent decades due to its diverse applications, we cite as examples the adsorption of amino acids (Misra *et al.*, 1997), proteins such as native lysozyme (Akazawa *et al.*, 1996) and succinylated lysozyme (Barroug *et al.*, 1997). Apatite can be combined with a variety of bioactive molecules, including anti-inflammatory, antimicrobial, antioxidant, and anticancer drugs (Jerdioui *et al.*, 2022) to create promising DDSs to directly treat infected bone tissue (Munir et al., 2021). Apatite has attracted more attention as a drug delivery system (DDS) for local and controlled release of biologically active compounds (Lara-Ochoa *et al.*, 2021). In this work, we synthesize a new phosphocalcic biomaterial with an apatitic structure containing oxygen species, with the chemical formula $Ca_{10}(PO_4)_6(OH)_2O_2$. This oxygenated apatite (OA) has antiseptic properties that can limit bacterial proliferation and provide continuous protection if the material remains in the implantation site. The oxygen released from OA as the bone regenerates can increase the local partial pressure of oxygen and inhibit anaerobic bacteria (Claude *et al.*, 1993) **(scheme 1)**. The studies concerning the preparation of OA are very limited. The first synthesis of OA was reported by Simpson in 1969, by treating β type calcium phosphate with 110 volume of oxygenated water (Simpson *et al.*, 1969). In 1989, Rey et al. patented an OA synthesized from a solution of $CaCl_2/H_2O_2$ and a solution of $(NH_4)_2HPO_4/H_2O_2$ (Rey *et al.*, 1989). An OA was synthesized in 2002 by a new process by mixing calcium hydroxide ($Ca(OH)_2$) with orthophosphoric acid (H_3PO_4) and hydrogen peroxide (H_2O_2) (Ansari *et al.*, 2002). In 2008, S. Belouafa et al. prepared OA crystallized under the physiological conditions of 37 °C and pH 7.4 by the reaction and precipitation of phosphate and calcium solutions. In this case, the calcium solution was prepared by dissolution of a calcium salt ($CaCO_3$, $Ca(NO_3)_2$ or $CaCl_2$) in hydrogen peroxide 30%. The phosphate solution was prepared by adding phosphoric acid to a solution oxygenated water 30% (Belouafa *et al.*, 2008). In 2013, an OA was prepared by controlling hydrolysis of dicalcium phosphate dihydrate or brushite, with a solution of oxygenated water. This apatitic matrix is a non-stoichiometric apatite that has several advantages, such as the purity of the final stage, a nanometric structure and a well-controlled and beforehand selected rheology (Lamhamdi *et al.*, 2013). Vandecandelaere and his collaborators extended the work of Simpson (Vandecandelaere *et al.*, 2013) on the synthesis of OA. Also, Yahyaoui et al. synthesized OA from the hydrolysis of cured brushite cement in aqueous medium, obtaining an apatite that contains both molecular oxygen and peroxide ions, which can be removed by heating the final product at about 300 °C (Yahyaoui *et al.*, 2014). Naanaai *et al.*, (2019) studied the influence of four factors such as reaction temperature medium, pH, hydrogen peroxide concentration and the mass of the hydroxyapatite attacked, as well as their interactions on the insertion rate of molecular oxygen into the apatitic tunnels. Inspired by these research results and considering the advantages of this apatitic

matrix (AO), we studied the synthesis and characterization of OA at different initial Ca/P ratio (1.67, 1.65, 1.63, 1.6, and 1.57) in the reaction medium. The objective of this study is to evaluate the effect of the Ca/P atomic ratio variations on the chemical and structural composition of the synthesized apatitic materials as well as on the quantity of molecular oxygen retained in their tunnels.

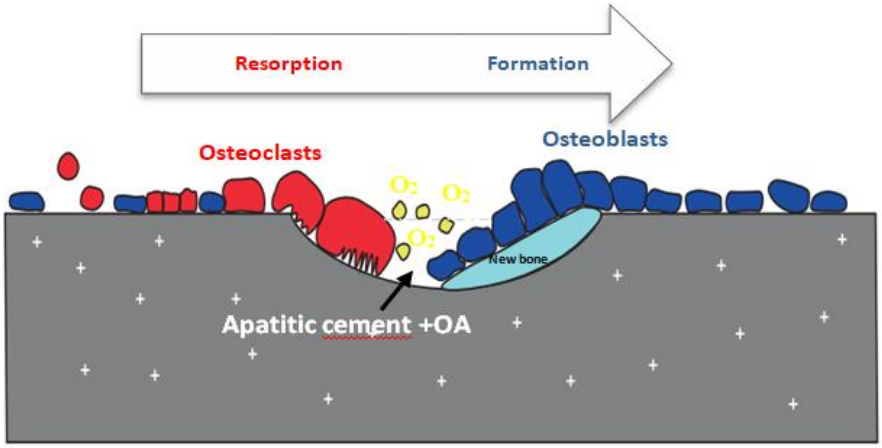

Scheme 1. Schematic illustration of the resorption of oxygenated apatite with the release of molecular oxygen.

2. Methodology

2.1. Preparation of apatites doped with molecular oxygen (OA)

The synthetic method used in this work to elaborate OA is the neutralization of freshly prepared, CO_2 removed $Ca(OH)_2$ milk of lime with dilute phosphoric acid H_3PO_4. A measured quantity of oxygenated water (10% [H_2O_2]) was mixed with the calcium oxide. Using a burette, a dilute solution (H_3PO_4 + 10% [H_2O_2]) was added drop wise and onto the walls of the beaker **(Scheme 2)**. The reaction mixture was kept under vigorous stirring for the duration of the reaction (2 h), and the final pH of the medium was 9.5. The product was then filtered, dried, and then calcined at 300 °C. Different OA were thus synthetized with different Ca/P ratios (1.67, 1.65, 1.63, 1.6, and 1.57) introduced into the reaction medium. The reaction involved is as follows:

$$a\ Ca(OH)_2 + b\ H_3PO_4 \xrightarrow{10\%\ [H_2O_2]} Ca_a(PO_4)_b(OH)_2O_2\ ;\quad (a/b=1.67,1.65,\ 1.63,\ 1.6,\ \text{and}\ 1.57).$$

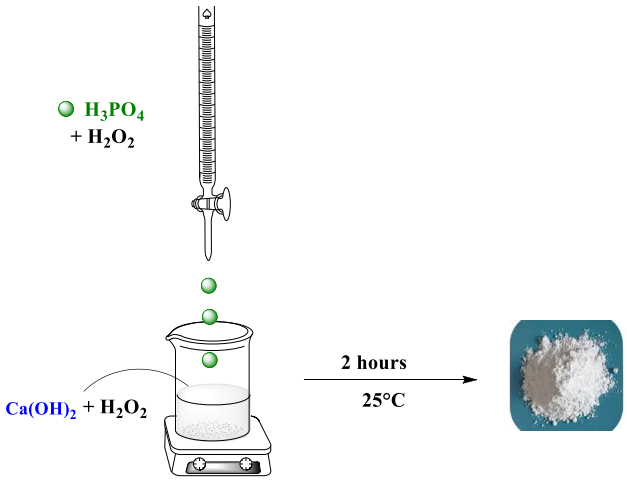

Scheme 2. Preparation of oxygenated apatite using neutralization reaction

The products obtained had a light-yellow color. They were then heated at 300 °C for 2 h to transform the peroxide ions into molecular oxygen. The final products had a white color, indicating the decomposition of the peroxide ions within the lattice, and the retention of the molecular oxygen in the apatitic tunnels (Kazen *et al.*, 2012; Rey *et al.*, 1972). All reagents used in the present work were received from Sigma Aldrich (Germany) and utilized without further purification.

2.2 Product characterization

The prepared samples were characterized by Fourier transform infrared spectroscopy (FTIR) using a Schimadzu FT-IR 8400S series instrument (Shimadzu Scientific Instruments, Japan). FTIR spectra were acquired over the region 400–4000 cm^{-1} in pellet form for 1 mg powder samples mixed with 200 mg spectroscopic grade (KBr). The structure of the samples was evaluated by X-ray diffraction (XRD) using a Shimadzu (XRD Shimadzu 6000) diffractometer with Cu-Kα radiation (1.5418 A˚). The thermogravimetric analysis was carried out by means of an apparatus of the type of Shimadzu DTG-60 simultaneous DTA-TG, with a speed of 10 °C/min and a temperature domain ranging from 25 to 1000 °C. The proportioning of the molar ratio Ca/P was carried out by method ICP–AES, by nebulizing and drying the liquid samples into solid aerosols under an argon flow, which transported them directly to the core of the plasma torch for atomization. The concentration calibration was performed with reference solutions prepared with a background salt. The specific surfaces were measured by BET (Brunaur, Emmett, Teller) and BJH (Barret, Joyner, Halenda) methods using an Autosorb-1instrument. The samples were degassed under secondary vacuum for an average of 12 h at 70 °C. The gas used in our study was a nitrogen with a molecular mass 28,013 g, across section of 16,200 A^2 and a liquid density of 0.808 g/cc. The measurements were performed at 77 K.
The morphology observation of the prepared OA was performed by scanning electron microscopy (SEM). To minimize the effects of load and achieve a resolution of 20 microns, we worked under low voltage (5 kV). Prior to be analyzed, the powders were deposited onto an adhesive patch of carbon. The molecular oxygen contained in the OA wa determined by volumetry. A mass of 0.5 g of OA was introduced into the flask. 6 ml of the perchloric acid contained in the bromine bulb was poured onto the OA. This released molecular oxygen and carbon dioxide trapped in the apatite tunnel. The volume of molecular oxygen released was measured using a U-tube filled with mercury. To measure the carbon dioxide, it was necessary to trap this element in the sodium hydroxide solution, and then to determine the number of moles of this element that exists in the OA, we measure this sodium hydroxide solution with hydrochloric acid (Jarcho *et al.*, 1981).

3. Results and Discussion

3.1 Analysis by FTIR spectroscopy

The FTIR absorption spectroscopy analysis **(Figure 1)** showed that all the products prepared had evolved into an apatitic phase. In addition, the band located between 1350 and 1500 cm^{-1}, which is characteristic of carbonate ions, showed some apatites that are slightly carbonated (Azzaoui *et al.*, 2019). For the apatitic products prepared with different initial Ca/P ratios initially in the reaction media, we observed a decrease in the intensity of the bands located between 1046-1087 cm^{-1} and 3000-3500 cm^{-1} as the Ca/P ratio decreases. These bands correspond respectively to the antisymmetric elongations of the PO_4^{3-} groups (Lakrat *et al.*, 2020) and to the water molecules adsorbed on the surface of the OA samples (Lakrat *et al.*, 2021).

3.2 X-ray diffraction characterization

Figure 2a showed the X-ray diffraction spectra of the products obtained with different Ca/P ratios and calcined at 300 °C. The XRD analysis of the synthetic products confirmed that they all had a poorly crystallized apatitic phase. After calcination of the synthesized products at 900 °C **(Figure 2b),** we obsereved the formation of a new phase of tricalcium phosphate (β-TCP) mixed with the apatite. The proportion of β-TCP increased as the Ca/P ratio decreased. The final pH of the reaction medium also decreased proportionally with the Ca/P atomic ratio, reaching the value of 7.6 for Ca/P = 1.57. The lower pH during the synthesis of apatite promoted the formation of β-TCP at the expense of the desired non-stoichiometric apatites. It is also possible that the β-TCP phase resulted from thermal decomposition of a non-stoichiometric phosphocalcic oxygenated apatite present at low temperature (Gibson *et al.*, 2000) (Raynaud *et al.*, 2002)

$$Ca_{10-x}(HPO_4)_x(PO_4)_{6-x}(OH)_{2-x} \longrightarrow (1-x)\ Ca_{10}(PO_4)_6(OH)_2 + 3xCa_3(PO_4)_2 + xH_2O$$

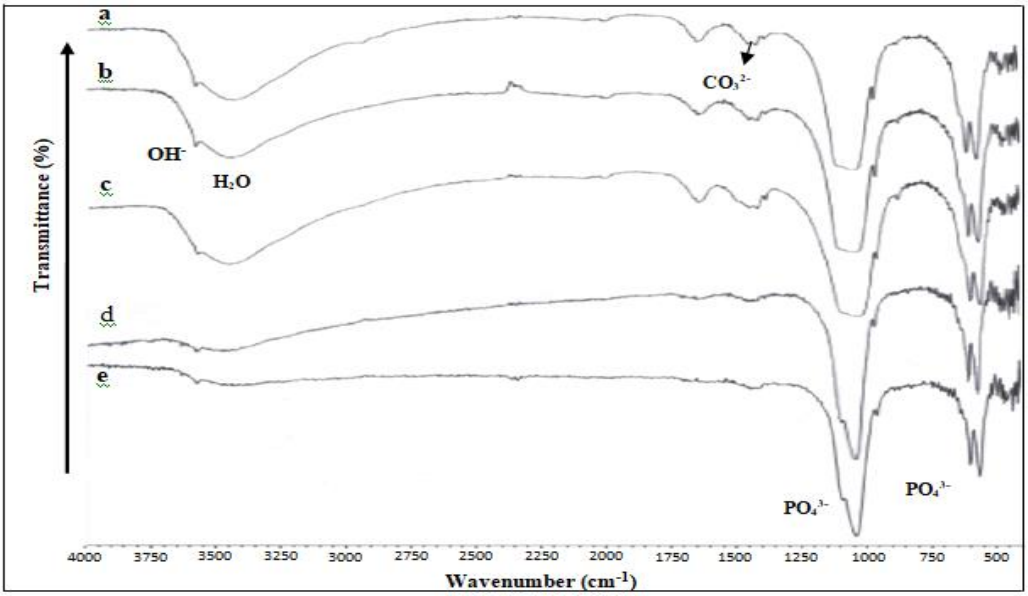

Figure 1. Infrared absorption spectrum (FTIR) of different Ca/P ratios calcined at 300 °C. (a: 1.67, b: 1.65, c: 1.63, d: 1.6, and e: 1.57).

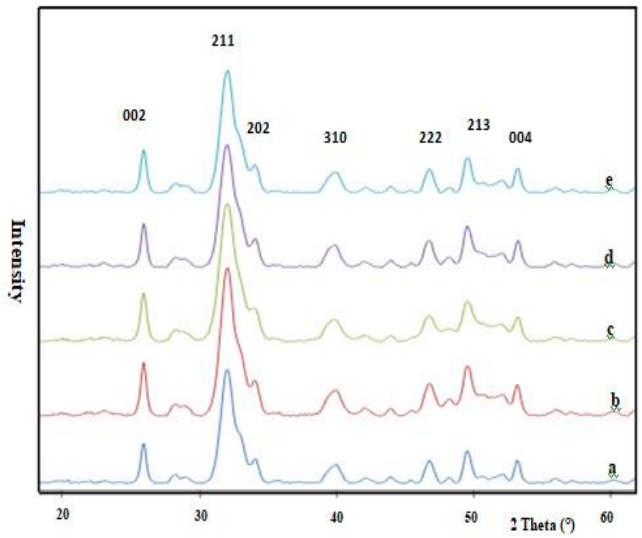

Figure 2a. DRX of different Ca/P ratios calcined at 300 °C. (a): 1.67, (b): 1.65, (c): 1.63, (d): 1.6 and (e): 1.57.

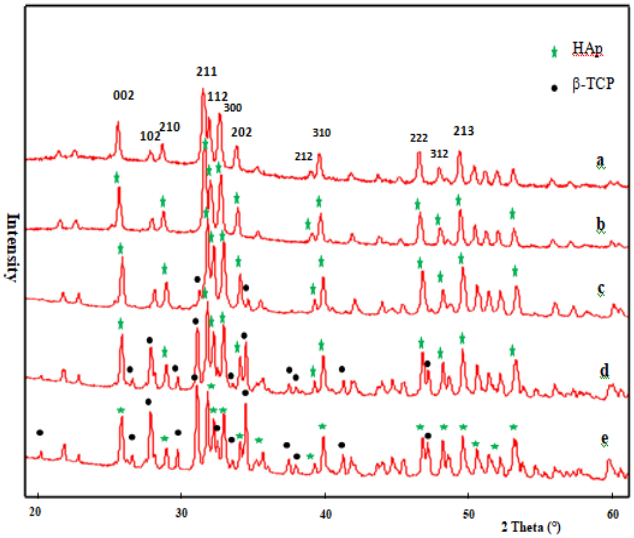

Figure 2b. DRX of different Ca/P ratios calcined at 900 °C. (a): 1.67, (b): 1.65, (c): 1.63, (d): 1.6 and (e): 1.57.

3.3 Thermogravimetric assessment and differential thermal analysis

The mass loss and the thermal variations of the OA (Ca/P=1.67) were monitored by TGA and DTA from room temperature to 1000 °C under a stream of nitrogen and with a heating rate of 10 °C/min. The TGA curve **(Figure 3a)** showed two mass losses which were very small at the beginning of the thermogram and at 600°C. The first mass loss was attributed to the desorption of water from AO surface. While the second loss corresponded to the elimination of residual carbonates (type A) detected by infrared spectroscopy at 1450 cm^{-1} (Choi *et al.*, 2017; Destainville *et al*, 2003; Raynaud *et al.*, 2002). The substitution possibility of OH^- (hydroxyapatite type A) and/or PO_4^{3-} (hydroxyapatite type B) groups by the carbonate ion (CO_3^{2-}) was described in the literature (Wallays *et al*, 1954). The DTA curve relating to the porous apatite **(Figure 3b)** showed the presence of two exothermic effects occurring at 50 °C and above 450 °C. These effects corresponded respectively to the removal of water molecules adsorbed on the surface of this material and the elimination of carbonate ions. The same results were observed for the other Ca/P ratios, indicating that the apatites were thermally stable.

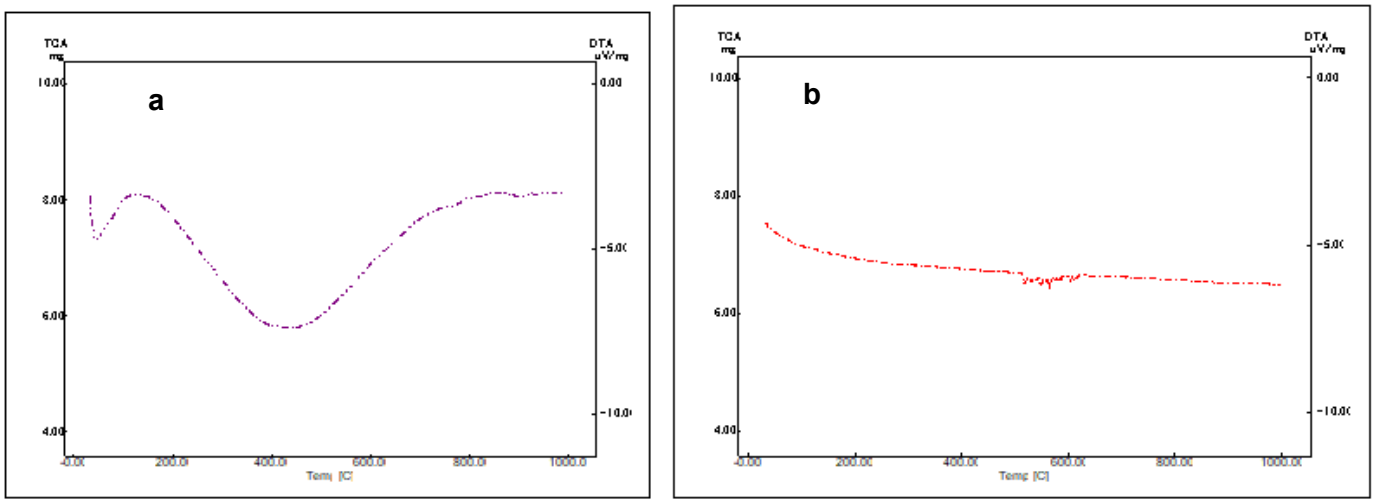

Figure 3. Thermogravimetric **(a)** and differential thermal analysis **(b)** of oxygenated apatite - Ca/P=1.67

3.4. Chemical analysis

The results of the chemical analyses of the prepared products were presented in **Table 1**. We noted that: For the sample series, the results of the Ca/P ratio measurements were in good agreement with those initially introduced. The variation in Ca/P ratios from 1.73 to 1.53 can be explained by the formation of a non-stoichiometric phase with calcium defects or by a two-phase AO/TCP mixture.

Table 1. Calcium, phosphorus, and measured Ca/P ratio of the oxygenated apatite of the various experimental Ca/P samples.

Sample	Ca (mg/L)	P (mg/L)	Ca/P
Ca/P = 1,67+10% H_2O_2	*332,5*	148,52	1,73
Ca/P = 1,65+10% H_2O_2	*336,3*	152	1,71
Ca/P = 1,63+10% H_2O_2	*337,8*	157,3	1,66
Ca/P = 1,6+10% H_2O_2	*326,4*	160,7	1,57
Ca/P = 1,57+10% H_2O_2	*330,2*	166,9	1,53

3.5. Description of the adsorption-desorption isotherms s

The adsorption-desorption isotherms of N_2 on OA of different Ca/P ratios were shown in **Figure 4a**. We noted that the adsorption isotherms of N_2 on the OA of different Ca/P ratios had a similar shape, with a hysteresis loop starting at a relative pressure P/P_0 = 0,73. The existence of a hysteresis suggested the presence of mesopores on the surface of the OA studied, where capillary condensation occurred. These isotherms N_2 adsorption-desorption are type IV according to the IUPAC classification (El-Hammari *et al.*, 2007; Yahyaoui *et al.*, 2014). The results of the measurement of the specific surface (SS), the pore volume (Vp), and the mean pore diameter (Dp) of the prepared OA were given in **Table 2**. The analysis of these results revealed that the specific surface area decreased as the Ca/P ratio increased slightly; it varied from 156.3 to 141.7 m^2/g. This was consistent with and the formation of more porous apatite as the deviation from stoichiometry increased. The pore size distribution curves of OA - Ca/P = 1.67 and OA - Ca/P = 1.57 were shown in **Figure 4b**. The pore size distribution of the prepared (A revealed the appearance of several populations of pores with diameter ranging from 3 to 40 nm. The number of pore populations varied as a function of the Ca/P ratio with a maximum at 10, 10.8, 8.9, 11.3, and 8.9 nm, respectively, for the OA - Ca/P (1.67, 1.65, 1.63, 1.6, and 1.57) **(Table 3)**. A comparison between all the synthesized OA clearly showed that the presence of molecular oxygen in the prepared solids had a significant influence on the pore size distribution and consequently on the specific surface area of the OA.

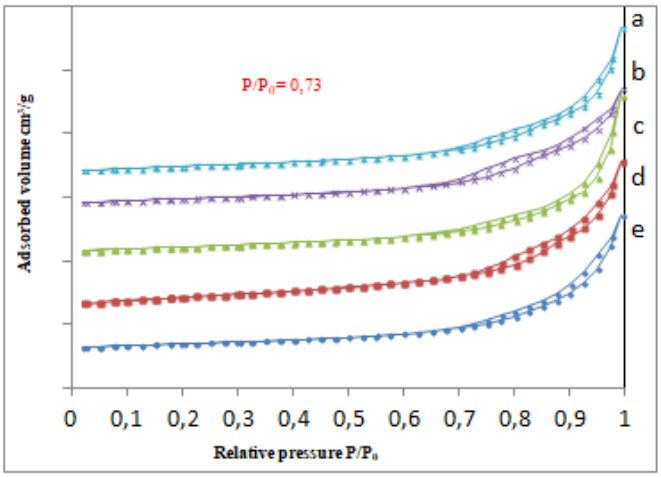

Figure 4a. Adsorption-desorption isotherms of N_2 on the AO of the different ratio Ca/P calcined at 300°C. (a): 1.57, (b): 1.6 , (c): 1.63, (d): 1.65 and (e): 1.67.

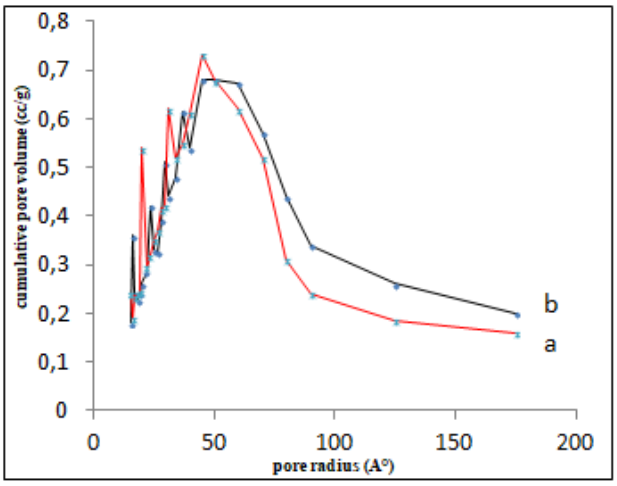

Figure 4b. Volume distributions of OA pore sizes for different Ca/P ratios. (a): 1.57, (b) 1.67.

Table 2. Volumetric analysis of oxygenated apatites - effect of the Ca/P ratio

Sample	Specific surface (m^2/g)	Pore volume (cc/g)	Rays of the pores (A)
Ca/P = 1,67+10% H_2O_2	141.659	0.686	50.207
Ca/P = 1,65+10% H_2O_2	152.514	0.664	54.70
Ca/P = 1,63+10% H_2O_2	156.247	0.795	44.811
Ca/P = 1,6 +10% H_2O_2	157.632	0.592	56.624
Ca/P = 1,57+10% H_2O_2	156.300	0.731	44.821

Table 3. Determination of the pore volume distribution as a function of the pore diameter of oxygenated apatites - effect of the Ca / P ratio

A.O-1.67-		**A.O-1.65-**		**A.O -1.63-**		**A.O-1.6-**		**A.O-1.57-**	
Dp (A°)	VP (cc/g)	Dp (A°)	VP (cc/g)	Dp (A°)	VP (cc/g)	Dp (A°)	VP (cc/g)	Dp (A°)	VP (cc/g)
32.1	0.36	31.4	0.72	32	0.6	40	0.3	40	0.54
46.4	0.42	46	0.58	50	0.64	56	0.37	64	0.62
56.8	0.508	66	0.54	68	0.72	113.2	0.59	89.6	0.73
75	0.618	108	0.675	89.6	0.795	***	***	***	***
100.4	0.68	***	***	***	***	***	***	***	***

3.6. SEM analysis

Figure 5a and **Figure 5b** visualized the morphology and distribution of the grains. We noticed that the OA particles were divided into two categories: one with large grains and the other with small ones. The examination of these aggregates showed that OA was made by particles of different sizes ranging from 6 to 15 µm. The particle size decreased when the Ca/P ratio decreased. The same conclusions are indicated by several researchers (Tornos *et al.* 2023; Belouafa *et al.* 2022; Lacerda Silva *et al.* 2020; Jerdioui *et al.* 2015)

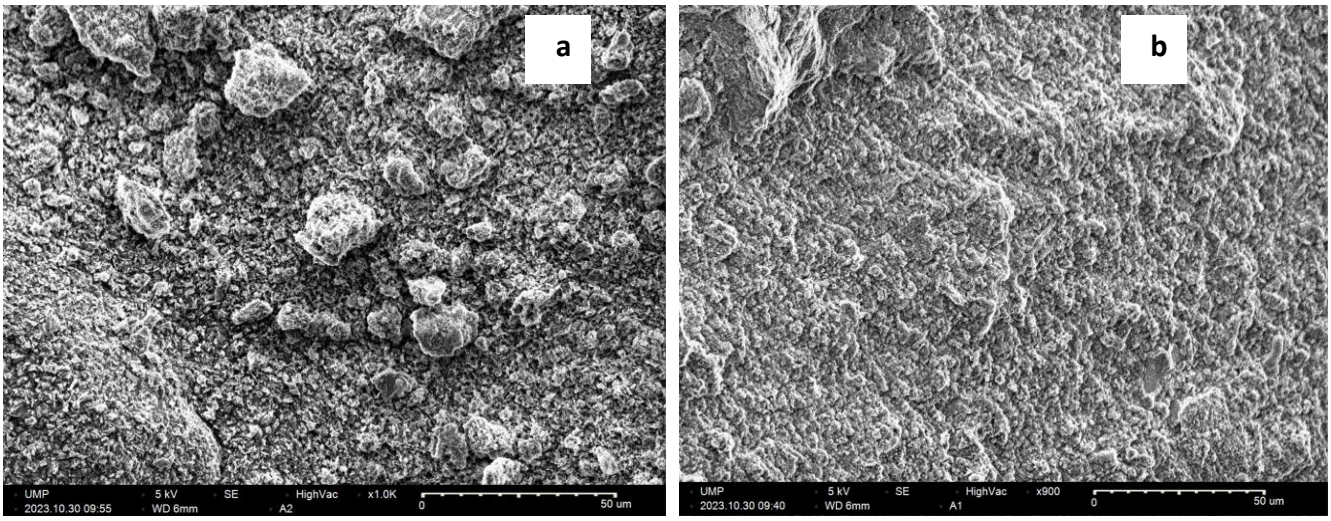

Figure 5. Scanning electron microscopy images of the oxygenated apatite calcined at 300 °C (**a**: Ca/P=1.67 ; **b**: Ca/P=1.57).

3.7. Variation of the oxygen content as a function of the Ca/P ratio

The results of the measurements of $n(O_2)$, $n(CO_2)$, and the derived chemical formulas of OA were given in **Table 4**. **Figure 6** indicated the variation of the molecular oxygen content as a function of the Ca/P ratio. It showed that the maximum insertion of O_2 was reached for Ca/P = 1.65, with a value of $3.5x10^{-4}$ mole. When the Ca/P ratio decreased, the rate of inserted oxygen decreased, reaching a very low value of $0.24x10^{-4}$ mol for Ca/P = 1.57. It's noted that Carbon, oxygen and sulfur are used to reconstruct the oxygenation stages of the sediments during organic matter degradation and precipitation of apatite (Su *et al.* 2023; Belouafa *et al.* 2022; Wudarska *et al.* 2022; Ibrahim *et al.* 2020; Ptáček, 2016; Jerdioui *et al.* 2015).

Table 4. n (O2), n (CO2), and Chemical formula of oxygenated apatite for different Ca/P ratios.

Ca/P ratio	$n(O_2)$ mole	$n(CO_2)$ mole	Chemical formula	Molecular oxygen content (% in weight)
1,67	$2,7\ 10^{-4}$	$6,3\ 10^{-6}$	$Ca_{10}(PO_4)_6(OH)_2(O_2)_{0,53}(CO_3)_{0,01}$	1,7
1,65	$3,5\ 10^{-4}$	$6,2\ 10^{-6}$	$Ca_{9,9}(PO_4)_6(OH)_2(O_2)_{0,69}(CO_3)_{0,01}$	2,24
1,63	$2,8510^{-4}$	$5,1\ 10^{-6}$	$Ca_{9,78}(PO_4)_6(OH)_2(O_2)_{0,56}(CO_3)_{0,01}$	1,8
1,6	$0,8\ 10^{-4}$	$2,4\ 10^{-6}$	$Ca_{9,6}(PO_4)_6(OH)_2(O_2)_{0,16}(CO_3)_{0,005}$	0,5
1,57	$0,24\ 10^{-4}$	$0,3\ 10^{-6}$	$Ca_{9,42}(PO_4)_6(OH)_2(O_2)_{0,05}$	0,15

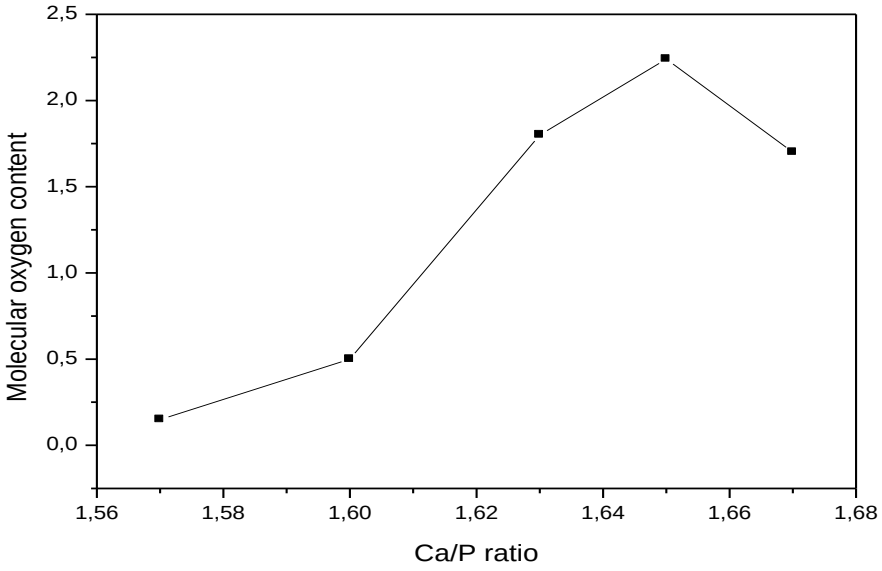

Figure 6. Variation of the molecular oxygen content as a function of the Ca/P ratio.

Conclusion

Oxygenated phosphocalcic apatites are of great interest in the field of orthopedic and dental surgery, due to the presence of molecular oxygen inserted in the apatite tunnels. The present study evaluated the effect of the variation in the Ca/P atomic ratio initially introduced in the reaction medium on the chemical and structural composition of the synthesized apatitic materials. The synthesis method used is the neutralization of freshly prepared, CO_2 free lime milk ($Ca(OH)_2$ + 10% [H_2O_2]) with a dilute phosphoric acid solution (H_3PO_4 + 10% [H_2O_2]). The results obtained showed the formation of a poorly crystallized apatitic phase, which became more crystalline after calcination at 900 °C. However, for a Ca/P ratio ≤ 1.60 a mixture of β-TCP and apatite was formed, with the proportion of β-TCP ratio increasing as the Ca/P ratio decreased. The thermal analyzes (TDA and TG) showed that the prepared phases underwent two mass losses, a first one very low at 50 °C, corresponding to the departure of water molecules adsorbed by the apatite, and a second one around 450 °C, corresponding to the departure of CO_2. The Ca/P ratio initially introduced influenced the quantity of O_2 inserted into the apatite tunnels, with a Ca/P ratio = 1.65 being the optimal value for better O_2 insertion. The chemical analyzes confirmed the preparation of non-stoichiometric phases. The specific surface reached a maximum value of 157.6 m^2/g, and it varied inversely with the Ca/P ratio of apatite. Our study provides a novel insight into the synthesis and characterization of OA with

different Ca/P ratios. However, we acknowledge that our work is not exhaustive, and there are still some open questions, such as the optimal conditions for oxygen insertion, the stability of oxygenated apatite in physiological environments, and the biological response of osteoblasts and bacteria to oxygenated apatite. We suggest that future research should focus on these aspects and evaluate the feasibility of using OA as a biomaterial for bone repair and protection.

References

Aaddouz M., Azzaoui K., Akartasse N., Mejdoubi E., Hammouti B., Taleb M., Sabbahi R., Alshahateet S. F. (2023). Removal of methylene blue from aqueous solution by adsorption onto hydroxyapatite nanoparticles, *Journal of Molecular Structure*, 1288, 135807. doi.org/10.1016/j.molstruc.2023.135807

Akartasse N., Mejdoubi E., Razzouki B., Azzaoui K., Jodeh S., Hamed O., Ramdani M., Lamhamdi A., Berrabah M., Lahmass I., Jodeh W., El Hajjaji S. (2017). Natural product-based composite for extraction of arsenic (III) from wastewater, *Chemistry Central Journal.* 1(11) 33. doi:10.1186/s13065-017-0261

Akazawa T., Kobayashi M., Kanno T., Kodaira K. (1996). Discrimination of Albumin and Lysozyme-Adsorption Characteristics on Two Differently-Originated Apatites, *Chemistry Letters*, 25(9), 779–780. doi:10.1246/cl.1996.779

Ansari L L., Elgadi M., Essaddek A., Mejdoubi E., (2001) Process for obtaining oxygenated apatite, Application to dental filling, Moroccan Office of Industrial and Commercial Property, Patent, 25548 [26552], Casablanca 01/01 / 2001.

Azzaoui K., Mejdoubi E., Lamhamdi A., Lakrat M., Hamed O., Jodeh S., Berrabah M., Elidrissi A., El Meskini I., Daoudi M. (2019) Preparation of hydroxyapatite biobased microcomposite film for selective removal of toxic dyes from wastewater, *Polymer* 1 (27) 28.

Barroug A., Fastrez J., Lemaitre J., Rouxhet P. (1997) Adsorption of Succinylated Lysozyme on Hydroxyapatite, *J. Colloid interface Sci*, 189, 37. https://doi.org/10.1006/jcis.1997.4787

Belouafa S., Hassan Chaair and Khalid Digua (2022) Oxygenated Apatites: Effect of Calcium Salt Nature and Synthesis Parameters, *Der Pharma Chemica*, 14, Issue 4, 26-33.

Belouafa S., Chaair H., Loukili H., Digua K., Sallek B. (2008) Characterization of Antiseptic Apatite Powders Prepared at Biomimetics Temperature and pH, *Materials Research*, 11, No. 1, 93-96.

Choi S. G., Park S. S., Wu S., Chu J. (2017) Methods for calcium carbonate content measurement of biocemented soils, *J. Mater. Civ. Eng.* 29 (11), 06017015.

Claude L., Edmond B., Lacout J.L., Rey C. (1993) biomaterial for osseous or dental filling and process for its preparation, EP0422719.

Destainville A., Champion E., Assollant D. B., Laborde E. (2003). Synthesis, characterization and thermal behavior of apatitic tricalcium phosphate, *Materials Chemistry and Physics*, 80, 269-277.

Dorozhkin S. V., (2019) Dental applications of calcium orthophosphates (CaPO4), *J. Dent. Res.* 1 (2) 1007.

El-Hammari L., Merroun H., Coradin T., Cassaignon S., Laghzizil A., Saoiabi A. (2007). Mesoporous hydroxyapatites prepared in ethanol–water media: Structure and surface properties, *Mater. Chem. Phys.* 104, 448–453.

El Hammari L., Latifi S., Saoiabi S., Azzaoui AK., Hammouti B., Chetouani A., Sabbahi R., (2022). Toxic heavy metals removal from river water using a porous phospho-calcic hydroxyapatite. *Moroccan Journal of Chemistry*, 10(1), 10–072. https://doi.org/10.48317/IMIST.PRSM/morjchem-v10i1.31752

Errich A., Azzaoui K., EL Hajjaji S., Mejdoubi E., Hammouti H., Abidi N., Akartasse N., Benidire L., Sabbahi R., Lamhamdi A., (2021) Toxic heavy metals removal using a hydroxyapatite and hydroxyethyl cellulose modified with a new Gum Arabic. *Indonesian Journal of Science & Technology*, 6(1), 41-64. https://doi.org/10.17509/ijost.v6i1.31480

Fiume E., Magnaterra G., Rahdar A., Verne E., Biano F. (2021) Hydroxyapatite for biomedical applications: a short overview, *Ceramics*, 4, 542-563. doi.org/10.3390/ceramics4040039

Gibson I R., Rehman I., Best S M., Bonfield W. (2000). Characterization of the transformation from calcium deficient apatite to β-tricalcium phosphate, *J. Mater. Sci-Mater. M*, 11(12), 799-804.

Ibrahim M., Labaki M., Giraudon J-M., Lamonier J-F. (2020). Hydroxyapatite, a multifunctional material for air, water and soil pollution control: A review, *Journal of Hazardous Materials,* 383, 121139, ISSN 0304-3894, https://doi.org/10.1016/j.jhazmat.2019.121139

Jarcho M. (1981) Calcium phosphate ceramics as hard tissue prosthetics, *Clin. Orthop. Relat. Res.* 157, 259-78

Jerdioui S., Elansari L.L., Bouammali B. (2015) Study of cobalt adsorption on an oxygenated apatite surface, *J. Mater. Environ. Sci.* 6 (3) (2015) 852-860

Jerdioui S., Ansari L L., Jaradat N., Jodeh S., Azzaoui K., Hammouti B., Lakrat M., Tahani A., Jama C., Bentiss F. (2022). Effects of gallic acid on the nanocrystalline hydroxyapatite formation using the neutralization process, *Journal of Trace Elements and Minerals.* 2773-0506. doi.org/10.1016/j.jtemin.2022.100009

Kazin, P. E., Zykin, M. A., Dinnebier, R. E., Magdysyuk, O. V., Tretyakov, Y. D., & Jansen, M. (2012). An Unprecedented Process of Peroxide Ion Formation and its Localization in the Crystal Structure of Strontium Peroxy-Hydroxyapatite $Sr_{10}(PO_4)_6(O_2)_x(OH)_{2-2x}$. *Zeitschrift Für Anorganische Und Allgemeine Chemie*, 638(6), 909–919. doi:10.1002/zaac.201200041

Lacerda Silva P, Bustin RM. (2020) Significance and Distribution of Apatite in the Triassic Doig Phosphate Zone, Western Canada Sedimentary Basin. *Minerals*, 10(10), 904. https://doi.org/10.3390/min10100904

Lakrat M., Fadlaoui S., Aaddouz M., El Asri O., Melhaoui M., Mejdoubi E. M. (2020). Synthesis and characterization of composites based on hydroxyapatite nanoparticles and chitosan extracted from shells of the freshwater crab Potamon algeriense, *Prog. Chem. Appl. Chitin. Deriv*. 25, 132–142.

Lakrat M., Jabri M., Ansari L. L., Mejdoubi E. M., Alves M., Fernandes M. H., Santos C. (2021). Three-dimensional nano-hydroxyapatite sodium silicate glass composite scaffold for bone tissue engineering-a new fabrication process at a near-room temperature, *Mater. Chem. Phys.* 260, 124185.

Lamhamdi A. (2013). Elaboration of new phosphate matrices for odontological, environmental and industrial in using the maturation controlled and techniques of hydrolysis, Doctoral thesis, Mohammed I University, Morocco.

Lara-Ochoa S., Ortega-Lara W., Guerrero-Beltrán C. E. (2021). Hydroxyapatite nanoparticles in drug delivery: physicochemistry and applications, *Pharmaceutics* 13 (10), 1642.

Misra D N., (1997) Interaction ofortho-Phospho-l-serine with Hydroxyapatite: Formation of a Surface Complex, *J. Colloid interface Sci*, 194, 249. https://doi.org/10.1006/jcis.1997.5108

Munir M. U., Salman S., Javed I., Bukhari S. N. A., Ahmad N., Shad N. A., Aziz F. (2021) Nano-hydroxyapatite as a delivery system: overview and advancements, *Artif. Cells Nanomed. Biotechnol.* 49 (1), 717–727. DOI: 10.1080/21691401.2021.2016785

Naanaai L., Azzaoui K., Mejdoubi E., Lamhamdi A., Lakrat M., Jodeh S. (2019). Study and Optimization of Oxygenated Apatite Obtained by Dissolution-Reprecipitation of Hydroxyapatite in a Solution of Hydrogen Peroxide. *Chemistry Africa.* 3, 227–235, doi.org/10.1007/s42250-019-00100-y

Maia F.R., Correlo V.M., Oliveira J.M., Reis R.L. (2019). Natural Origin Materials for Bone Tissue Engineering: Properties, Processing, and Performance, *Principles of Regenerative Medicine (III),* 535-558 (32). doi.org/10.1016/B978-0-12-809880-6.00032-1

Ptáček, Petr. 2016. 'Substituents and Dopants in the Structure of Apatite'. Apatites and Their Synthetic Analogues - Synthesis, Structure, Properties and Applications. *InTech.* doi:10.5772/62213

Raynaud S., Champion E., Assollant., (2002). Calcium phosphate apatites with variable Ca/P atomic ratio I. Synthesis, characterisation and thermal stability of powders, *Biomaterials*, 23(4), 1065-1072

Rey C., (1972), 3 m Cycle Thesis, Toulouse.

Ledard C., Benque E., Lacaout J., Rey C. (1989). Biomaterials for bone or dental filling, and preparation processes. Patent Fr., 98, 13246.

Saidi N., Azzaoui K., Ramdani M., Mejdoubi E., Jaradat N., Jodeh S., Hammouti B., Sabbahi R., Lamhamdi A. (2022). Design of Nanohydroxyapatite/Pectin Composite from Opuntia Ficus-Indica Cladodes for the Management of Microbial Infections. *Polymers*, 14(20), 4446. doi.org/10.3390/polym14204446

Siddiqui H A., Pickering K L., Mucalo M R., (2018). A Review on the Use of Hydroxyapatite-Carbonaceous Structure Composites in Bone Replacement Materials for Strengthening Purposes, *Materials (Basel)*. 11(10), 1813. doi: 10.3390/ma11101813.

Simpson D. R. (1969) Oxygen-rich apatite, *Am. Miner*, 54, 560-562.

Su J-H., Zhao X-F., Hammerli J. (2023). Apatite CO_2 and H_2O as Indicators of Differentiation and Degassing in Alkaline Magmas, *Journal of Petrology*, 64(8), egad061, https://doi.org/10.1093/petrology/egad061

Subirade M., Lebugle A., (1991) Thermal decomposition of an apatitic phosphate containing an organic phosphate in its lattice. *Ann. Chim. Fr*, 16, 89.

Subirade M., Lebulge A., (1993) On the study of a mineralorganic interface between a calcium phosphate and a phospholylated monomer, *Ann. Chim. Fr*, 18, 183.

Tornos, F., Hanchar, J.M., Steele-MacInnis, M. et al. (2023) Formation of magnetite-(apatite) systems by crystallizing ultrabasic iron-rich melts and slag separation. *Miner Deposita*. https://doi.org/10.1007/s00126-023-01203-w

Vandecandelaere N., Bosc F., Rey C., Drouet C. (2014). Peroxide-doped apatites: Preparation and effect of synthesis parameters, *Powder Technology*. doi.org/10.1016/j.powtec.2013.09.015

Wallays R., (1954) C.R. Coll. Intern. Chim. Pure et appliqué Munster, westph, P.183.

Wudarska A., Wiedenbeck M., Słaby E., Lempart-Drozd M., Chris Harris, Joachimski M. M., Lécuyer C., MacLeod K.G., Pack A., Vennemann T., Couffignal F., Feng D., Glodny J., Kusebauch C., Mayanna S., Rocholl A., Speir L., Sun Y., Wilke F. D. H. (2022) Inter-laboratory Characterisation of Apatite Reference Materials for Oxygen Isotope Analysis and Associated Methodological Considerations, *Geostandards and Geoanalytical Research*, 46(2), 277-306

Yahyaoui R., Mejdoubi E., Azzaoui K., Lamhamdi A., Elabed S., Hammouti B. (2014). Preparation of oxygenated apatite from hydrolysis of cured brushite cement in aqueous medium. *Der Pharma Chemica*, 6(6), 133-138.

(2024) ; https://revues.imist.ma/index.php/morjchem/index